X-ray diffraction study of Anodisc filters

Michael R. Fisch, Andrew Primak, and Satyendra Kumar
Department of Physics and Liquid Crystal Institute, Kent State University, Kent, Ohio 44242-0001
(Received 30 October 2001; published 8 April 2002)

X-ray diffraction from Anodisc membrane filters is measured and analyzed. The patterns are consistent with pores of constant diameter and a Gaussian distribution of pore-pore spacing. The mean distance between pores, measured using x rays is 0.37 μm compared to 0.32 μm calculated from the nominal density of pores/cm^2. The results may be modeled both in terms of the convolution of a structure factor of the pores with the resolution function, and by modeling the source as a collection of incoherent sources with an ideal monochromator crystal. The incoherent source analysis provides an explanation for the common observation that the resolution function in many x-ray spectrometers is better fit to a sum of Lorentzians, rather than a single Lorentzian.

DOI: 10.1103/PhysRevE.65.046615 PACS number(s): 68.05.Cf, 68.18.Fg, 42.25.Bs

I. INTRODUCTION

The use of x-ray diffraction to study the structure of bulk materials, surfaces and layers has been well characterized and studied [1–3]. A few years ago, the diffraction patterns obtained from Anodisc^{TM} filters were examined [4] and it was suggested that simple diffraction phenomena were not totally responsible for the observed behavior. This paper will explain and analyze these spectra. In the process of analyzing these data, we investigated the effects of the coherence lengths, both longitudinal and transverse, of the x-ray beam on the measured spectrum. Typically, these lengths are much greater than any characteristic length of the objects being studied. For this reason, most analyses consider the x-ray source to be infinitely coherent. Alternatively, the source's coherence is not explicitly included in the analysis. Since measurements of quantities, such as critical exponents with different spectrometers and sources, yield essentially the same result, presumably this is not a serious problem in most experiments. However, the analysis of diffraction from Anodisc samples allowed a systematic study of a situation in which a coherence length of the incident x-ray beam is comparable to an independently determined characteristic size of a structure and an interstructure distance. This paper summarizes our results in this area, and shows how the spatial size of the source, and hence its coherence properties have been implicitly incorporated into standard analyses. We will also discuss how these coherence effects can be incorporated into analyses of diffraction patterns.

Anodisc membrane filters are distributed by the Whatman Company. They are made of aluminum oxide and are supplied with a nominal thickness of 60 μm. These filters are readily available with several different nominal pore sizes and provide a reproducible test platform for the measurements. In these filters, the pores are not circular in cross section and form a somewhat random honeycomb structure; however, the variation in the size of the pores is rather small and the distance between the pores is larger than a typical pore diameter. The pores are initially formed by bombardment of the membrane by α particles. The pores are then etched to the final cross-sectional area. Since the aluminum oxide substrate is generally polycrystalline, this etching will generally lead to pores that meander through the membrane. In the pores studied, the thickness of the membrane is 300–600 times the mean pore diameter so this meandering of the pores may have some secondary importance. However, the simplest explanation of the observed spectra is obtained by a model that has uniform sized pores, a Gaussian distribution of pore spacing, and a broad source that can be modeled by either a quasicoherent source or a resolution function. The dependence of the measured spectra on the pore diameter is small; therefore, variations of the pore diameter about the mean are not included in the model. Experimentally there is very little difference in the spectra from 0.1 and 0.2 μm pore sizes and simulations of model spectra largely confirm this result.

II. EXPERIMENTAL DETAILS AND RESULTS

The experiments were performed on samples at room temperature. The x-ray diffraction experiments were performed using a 12 kW Rigaku RU-200 rotating anode generator with a Mo target and a two-circle spectrometer. The unit was operated at a potential of 40 kV and a current of 20 mA. A pair of single Si (111) crystals was used as a monochromator and analyzer to select the Mo $K\alpha$ doublet. Because the measurements were made at very small scattering angles, the separation of the $K\alpha_1$ and $K\alpha_2$ lines was not analyzed. Two x-y slits with tantalum blades were placed after the monochromator crystal. These define the x-ray spot size and the out-of-plane (out of scattering plane) resolution. The corresponding longitudinal and transverse resolutions of our spectrometer are $\Delta q_{\|} \approx 2\times10^{-4}$ Å and $\Delta q_{\perp} \approx 3\times10^{-6}$ Å, respectively. The sample plane is approximately 2 m from the anode. Details of the experimental setup can be found elsewhere [5].

The arm-zero profile, which gives the fundamental longitudinal resolution of the spectrometer, can be fit to the sum of three Lorentzians. In this scheme, one Lorentzian is centered at zero scattering angle and the other two are symmetrically displaced by a small angle δ from zero angle. This empirical procedure has been commonly applied [6] and has the advantage of making convolutions with theoretical forms simpler than other schemes. However, there is no firm theo-

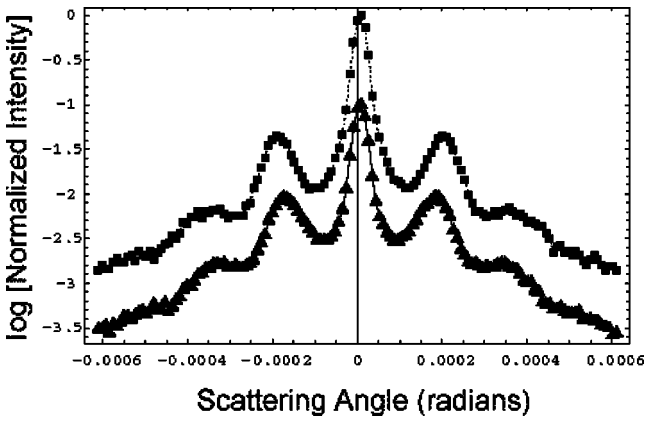

FIG. 1. Logarithm (base 10) of the normalized scatter intensity from a 0.1 μm pore diameter filter (top) and a 0.2 micron pore diameter filter vs scattering angle. The lower curve is displaced vertically by 1 unit.

retical basis for this form other than the significant observation that it yields a good fit, and it makes further data analysis significantly easier. Later, we will present a theoretical model that fits the data better than this model, and explains why the resolution function is not a single Lorentzian. The primary experimental results of this study are shown in Fig. 1.

The top of Fig. 1 is a graph of an experimental scan of an Anodisc filter of nominal pore diameter 0.1 μm. The central peak is resolution limited. The bottom spectrum in Fig. 1 shows the corresponding data for a 0.2 μm filter. Once more, the central peak is resolution limited. Both of these curves, when normalized to a peak value of 1.00 as shown are essentially identical. This result is surprising and indicates the need to carefully explore the origins of these scattering patterns. The following section of this paper will present a model that can be used to analyze these diffraction patterns.

III. MODELING OF DIFFRACTION PATTERNS—ANALYSIS OF THE DATA

The superposition of the diffraction patterns for two different pore sizes indicates that the phenomenon is subtler than diffraction from essentially isolated holes in a membrane [7]. This section will analyze the data using both an optical model and the more standard x-ray approach in which the measured spectrum is the convolution of the sample's structure factor and the resolution of the spectrometer. We will demonstrate that these two approaches are nearly equivalent and in the process demonstrate why the resolution of so many high-resolution x-ray spectrometers is well represented by the three Lorentzian model.

Two characteristic length scales describe these samples. The first is the linear dimension, or diameter, of an average pore. This is 0.1 or 0.2 μm; depending on the filter studied. The other length is the mean distance between the pores. This is larger than the pore size. The specifications of these membranes state that there are 10^9 pores per cm^2 of membrane [8]. Thus, the mean distance between the pores is the square root of the reciprocal of this number, 3.2×10^{-5} cm or 0.32 μm. This is smaller than that obtained by fitting the x-ray data. This value depended on the type of fit, and pore size, but is within 5% of 0.37 μm. Moreover, these two distances are larger, but not an order of magnitude larger than the two transverse coherence lengths of the x-ray beam.

A. Quasicoherent source analysis

The study of partially coherent sources in optics is well known; this section will apply some results from this area to the analysis of these x-ray diffraction experiments. Electromagnetic wave coherence is described in terms of coherence in the direction of propagation of the wave, the ''longitudinal coherence length,'' and transverse to the wave, the two ''transverse coherence lengths.'' Similar words have been used to describe the resolution of the x-ray spectrometer. When discussing the x-ray spectrometer these terms have different meanings. Transverse means perpendicular to the scattering vector and in the scattering plane. Longitudinal means within the scattering plane, parallel to the scattering vector. Finally, the direction perpendicular to the scattering plane is known as the ''vertical'' direction. To minimize confusion we will designate the electromagnetic wave coherence length in the scattering plane as the horizontal coherence length and the vertical coherence length the corresponding length perpendicular to the scattering plane.

The longitudinal correlation length of an electromagnetic wave is given by the expression [9] $l\approx(\overline{\lambda}/\delta\lambda)\overline{\lambda}$, where $\overline{\lambda}$ is the mean wavelength of the radiation and $\delta\lambda$ is the bandwidth of the radiation. For the Mo $K\alpha$ doublet this length is roughly 120 Å. While for either the $K\alpha_1$ or $K\alpha_2$ lines separately it is approximately 0.18 nm. This length is important in temporal interference experiments and is of no more concern in the present context [9,10].

The transverse coherence lengths of the beam are related to the spatial coherence of the x rays incident on the sample. These lengths reflect some of the properties of the effective source, such as its finite physical size and the fact that different parts of the source emit radiation of different phases. Our analysis of these lengths proceeds as follows. The portion of the anode that is struck by electrons from the filament is rectangular in area and is 0.5×10 mm^2. The exit ports (slits) are constructed so that this area is viewed at a take-off angle of approximately 6°. Thus, the ''footprint'' of the x-ray source is roughly 0.5×1 mm^2. This radiation is matched to an entrance slit of the monochromator by another slit of width less than 1 mm. The effective width of the slit will depend on the acceptance angle of the monochromator crystal and can be less than 0.1 mm. In the present experiment, the separation between the anode and the first slit is of 30 cm and the slit width is 1 mm. This corresponds to an angular variation $\Delta\theta$ of 3×10^{-3} rad. The energy width of the Bragg reflected x rays, assuming reflection from an ideal crystal, is limited by the collimation. It is expressed as $\Delta E=\Delta\theta E_{K\alpha}/\tan\theta_B$ eV$\approx$300 eV [11]. Here, E_{K_α} is the energy of either Mo $K\alpha$ x-ray line (in eV), and θ_B is the Bragg scattering angle for the Si (111) plane. This is substantially wider than the energy separation of the $K\alpha_1$ and $K\alpha_2$ lines (approximately 105 eV) and thus this slit is incapable of separating the $K\alpha_1$ and $K\alpha_2$ lines. The width of the beam is

set by the second set of slits after the monochromator crystal, and is less than 1 mm wide. The primary purpose of the monochromator crystal and two pairs of x-y exit slits is to reduce the bremstrahlung and lines other than $K\alpha$ radiation, and ensure a well-collimated beam.

In this analysis, the radiation from the anode is modeled as a maximally incoherent planar source of uniform illuminance and the monochromator crystal is assumed ideal. Thus, individual areas larger than approximately one wavelength of the x rays (0.07 nm) on a side are considered to be incoherent. By considering the anode as a collection of individual radiators, we may apply the Van Citter-Zernike theorem of optics to describe the propagation of mutual intensity from the source. The derivation of this theorem can be found in Ref. [12]. The important result of applying this theorem is that, apart from a phase factor and a scaling factor, the mutual intensity (which is collegially the intensity) is described by the two-dimensional Fourier transform of the source intensity distribution. From this result and the assumption of a uniformly bright incoherent source of area A_s, one obtains the following expression for the coherence area at a distance r from the source [13]: $A_{coherence} \approx (r\bar{\lambda})^2/A_s$. This can be represented as the product of the two transverse coherence lengths that are produced by an effective source of dimensions $l_{horizontal}$ and $l_{vertical}$ and expressed as follows: $A_{coherence} \approx (r\bar{\lambda}/l_{horizontal})(r\bar{\lambda}/l_{vertical})$. In the present situation $r \approx 2$ m, and assuming the source is the anode, A_s is a rectangle with sides estimated to be 0.5 mm wide and 1 mm high. Thus, the coherence area, roughly an area over which the beam may be considered coherent, is also a rectangle, whose longer coherence length is in the horizontal direction.

Using the source size discussed above as estimates, we find the vertical coherence length is roughly 70 nm, while the horizontal coherence length is roughly 140 nm. The modeling to be discussed in the following section as well as the secondary peaks in the spectra indicate that this horizontal coherence length is an underestimate. Notice that the vertical coherence length is similar to a typical pore diameter of 100 or 200 nm. For this reason, we anticipate that pores separated by significantly more than a vertical coherence length will be illuminated by incoherent x rays and do not contribute to coherent scattering and interference effects to the measured spectra.

Thus, our model will be simple. We treat the system as essentially one dimensional. This is a poorer approximation for the larger pores, as results of the modeling will indicate. Note also that the relative smallness of the horizontal coherence length means that neighboring pores in a single vertical plane are illuminated by a partially coherent x-ray beam. In the present model, the source will be treated as infinitely high and of variable width. The width of the source $2t$ will be treated as an adjustable parameter and will be adjusted to obtain a good match to the data. The sample (filter) will be modeled as long parallel slits of fixed width 0.1 or 0.2 μm with a mean center-to-center spacing modeled by a Gaussian distribution whose mean and standard deviations are varied to fit the data. The pore (slit) width is modeled as a constant since a 10% variation about the mean width had essentially no effect on the model spectrum.

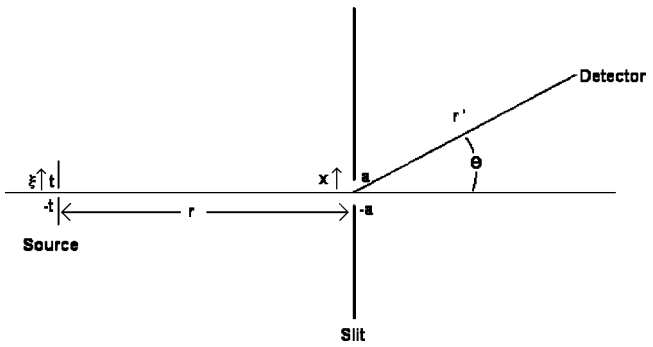

FIG. 2. Experimental geometry showing how the distances and coordinates are labeled.

The various coordinates and distances needed to model diffraction from a collection of parallel slits of width $2a$ and finite-sized source of width $2t$ is shown in Fig. 2. The distance between the source and the sample (that is now modeled as slits) is r. In the spectrometer, r' is sufficiently large and the pore sizes sufficiently small that the far-field approximations are valid. A line through the centers of both the source and the sample defines the ''zero angle.'' The scattering angle θ is measured from this line as shown in the figure. This angle is sufficiently small that in the following model $\sin\theta \approx \theta$. The coordinate that describes the position within the source is ξ, while the coordinate describing the position within the plane of the slits is x. The origin of these is the center of the source slit, and the center of the central slit in the sample.

Consider x rays produced in an infinitesimal part of the source of width $d\xi$ located at ξ. The x rays from this infinitesimal width will produce coherent scattering due to the slits. For a single slit in the sample plane the additional phase (beyond that of direct propagation) of the incident light at position x within the slit is

$$\exp\left(\frac{ikx\xi}{r}\right). \tag{1}$$

In this expression, k is the magnitude of the wave vector of the incident x rays, $2\pi/\lambda$. This incident radiation will be diffracted by the slit, causing another phase shift, given by

$$\exp(-ik\theta x). \tag{2}$$

Here, the approximation $\sin\theta \approx \theta$ has been made. The diffracted intensity of the whole slit due to this infinitesimal source is found, using scalar diffraction theory [14], by integrating over the slit and squaring the result,

$$dI(\theta) = \left[\int_{-a}^{a} \exp(-ikx\theta)\exp\left(\frac{ikx\xi}{r}\right)dx\right]^2 d\xi$$

$$= 4a^2\left[\frac{\sin[ka(\theta+\xi/r)]}{[ka(\theta+\xi/r)]}\right]^2 d\xi. \tag{3}$$

In this expression, for simplicity, overall constants have been set equal to unity. The intensity due to this single slit and the

whole incoherent source is found by integrating over the source that is modeled as an infinitely long slit of width $2t$,

$$I(\theta)=4a^2\int_{-t}^{t}\left[\frac{\sin[ka(\theta+\xi/r)]}{[ka(\theta+\xi/r)]}\right]^2 d\xi. \tag{4}$$

Alternate expressions in terms of the mutual intensity function are in Ref. [12]. Of course, the samples studied contain multiple pores. The effect of a series of slits is discussed in Ref. [14]. The previous solution, Eq. (4), is modified by including the appropriate interference term [15]. For N slits of fixed width $2a$ and spacing $2b$, one finds that

$$I(\theta)=4a^2\int_{-t}^{t}\left[\frac{\sin[ka(\theta+\xi/r)]}{[ka(\theta+\xi/r)]}\right]^2 \times\frac{1}{N^2}\left[\frac{\sin^2[Nbk(\theta+\xi/r)]}{\sin^2[bk(\theta+\xi/r)]}\right]d\xi. \tag{5}$$

Finally, allowing the pore spacing $2b$ to have a normalized Gaussian probability distribution, one can write $I(\theta)$ as a double integral over the source from $-t$ to t and the pore spacing, b as follows:

$$I(\theta)=4a^2\int_{-\infty}^{\infty}\frac{1}{\sqrt{2\pi\sigma^2}}\exp[-4(b-b_0)^2/2\sigma^2]db \times\int_{-t}^{t}\left[\frac{\sin[ka(\theta+\xi/r)]}{[ka(\theta+\xi/r)]}\right]^2 \times\frac{1}{N^2}\left[\frac{\sin^2[Nbk(\theta+\xi/r)]}{\sin^2[bk(\theta+\xi/r)]}\right]d\xi. \tag{6}$$

In this expression σ is the standard deviation of the probability distribution, and $2b_0$ is the mean value of the interslit spacing. The inclusion of a distribution of slit widths can be accomplished in a similar manner. This requires one more integration and correspondingly more computation time. This integral was evaluated by performing a numerical integral over b, and summing over ξ using values so small that the source could be considered coherent. The programs were implemented using MATHEMATICA. Both the simulated data and the experimental data indicate that the model and observed spectra are essentially independent of the slit width (or pore diameter), so no integration over this parameter was performed. A value of $N=20$ was used; increasing or decreasing N from this value had no effect on the simulated data.

By numerically calculating $I(\theta)$ one can obtain estimates of the slit (pore) width $2a$, the slit (pore) spacing $2b$, and the source width $2t$. This calculation assumes a finite source and the diffraction pattern is measured with infinite resolution; that is, we allowed the source to be the primary determiner of the resolution. This would appear to be a poor approximation given the resolution function illustrated by the experimental data as the central peak of the diffraction pattern. However, this is not the case, as the results will show. The standard analysis of this data consists of convoluting the sample structure factor (for infinite coherence length x rays) with the longitudinal resolution function of the spectrometer. This procedure will also yield a similar result.

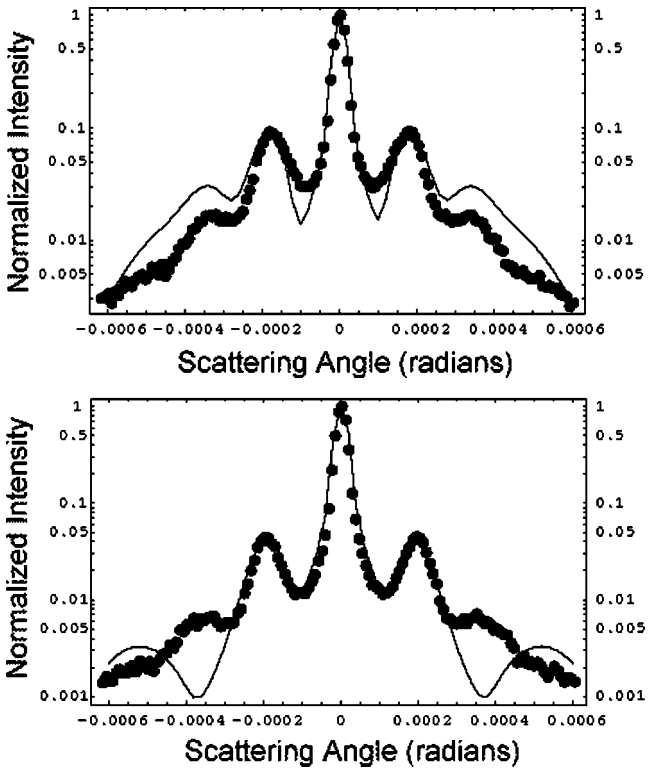

FIG. 3. Normalized experimental data (points) and fits (lines) from the model, Eq. (6) vs scattering angle. Top, 0.1 μm pore size; bottom, 0.2 μm pore size.

The size and width of the secondary maxima and the depth of the valley between the central maximum and these secondary peaks in the experimental data place a serious constraint on the coherence of the source. The source appears to be well modeled by a slit of width $2t$ mm as described by the experimental geometry and our model. However, modeling with source slits that are too wide leads to wider secondary peaks than are observed experimentally. Similarly, a very small source width leads to valleys that are significantly too shallow. By performing numerous simulations, we found that the effective source width is substantially smaller than 0.5 mm estimated from the x-ray anode, and is much better explained by a source of width 60 μm. This is consistent with the high quality Si monochromator crystal employed.

The calculated diffraction patterns, based on this model, are shown in Fig. 3. The calculation does not include any extra broadening of the diffraction features due to the spectrometer's resolution function. This figure shows the logarithm of the data and the model predictions on the same scale. In this figure, the model also includes a component of undiffracted x rays. This component represents approximately 80–90 % of the total intensity. While the simulations are not replicas of the experimental data, they show the essential correctness of the model and suggest its application to analysis of data. In addition, the model is less exact when wider slits are modeled. This is because the wider pores are

less well represented by an infinite slit with parallel sides. The 0.2-μm pore filters were fitted with a pore radius of 0.1 μm and a mean pore spacing of 0.35 μm. The 0.1-μm pore filters were fitted with a mean pore spacing of 0.39 μm. The effects of varying the width of the pore spacing distribution were studied. In both cases, $\sigma=2\times10^{-2}$ μm. It is found that the value of σ^2 of 0.0005 ± 0.0001 leads to good replication of the closest secondary maxima. It is significant to note that the simulations are not very sensitive to small variations in the source width $2t$. A variation of a factor of 2 leads to very little change in the model spectra.

The expression for the diffracted intensity as a function of scattering angle, Eq. (6), merits further analysis. This expression can be rewritten as

$$I(\theta)=A\int f(b)db\int_{-\infty}^{\infty}\Gamma(\xi,t)f(a,b;\theta+\xi)d\xi. \qquad (7)$$

Here $f(b)$ represents the Gaussian probability distribution, the diffraction and interference terms are written as $f(a,b;\theta+\xi)$ [this is shorthand for the integrand in Eq. (5)], $\Gamma(\xi,t)$ is a function that obtains the value 1 for $|\xi/t|\leqslant1$, and 0 otherwise, and A is a constant. Upon changing the order of integration, this form indicates that the diffracted intensity can be written as the convolution of the Gaussian averaged diffraction-interference term and a source function $\Gamma(\xi,t)$. This convolution is with the source term, not with resolution function. This form suggests that a more correct analysis of x-ray diffraction patterns would include a convolution of the structure factor with the source function. This will be discussed in the following section.

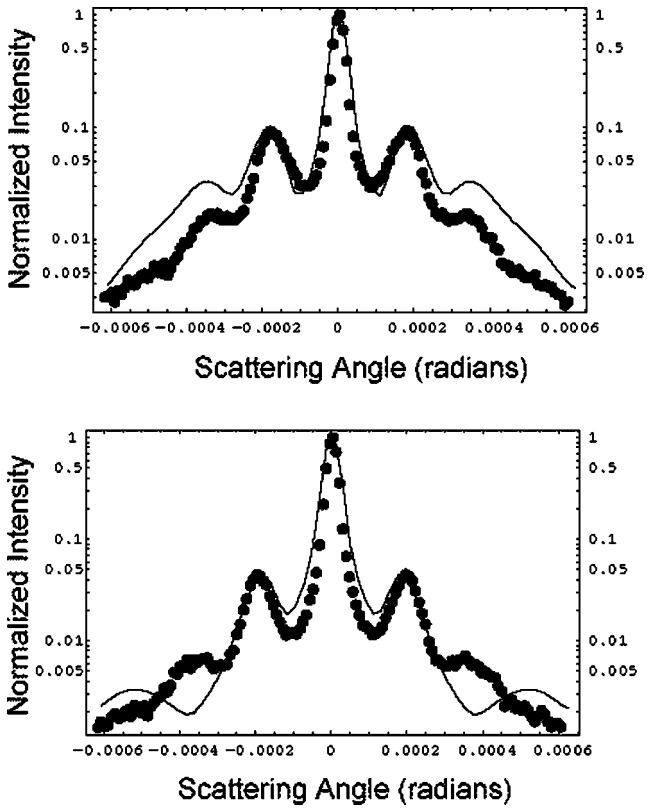

FIG. 4. Normalized experimental data (points) and fits (lines) from convoluting the resolution function with the sample structure factor. Top 0.1 μm pore filter, bottom 0.2 μm pore filter. The mean spacing between pores has been adjusted from those in Fig. 3 to yield better fits.

B. X-ray resolution function analysis

The standard analysis of high-resolution x-ray spectra begins with the observation that the measured intensity is proportional to the convolution of the sample's structure factor and the resolution function of the spectrometer. In this calculation, it is assumed that the source is perfectly coherent. It is further assumed that the resolution function can be separated into three spatial components and an energy component. Moreover, the energy resolution of the spectrometer is so broad that the spectrometer integrates over all energies in the dynamic structure factor yielding the zero-time, static structure factor. Applying these ideas to the present analysis, the measured intensity at a scattering angle θ can be written as

$$I(\theta)\propto\int R(\theta-\theta')S(\theta')d\theta'. \qquad (8)$$

In this expression, $S(\theta)$ is the static structure factor (diffraction pattern calculated for a coherent source) at scattering angle θ, and $R(\theta)$ is the longitudinal resolution function. The present discussion is in terms of the scattering angle rather than the more normal scattering vector q. These can be easily related through the expression $q=k\sin\theta$ when $\theta-2\theta$ scans are performed. In the present context, this means that an alternate mode of the analysis of these patterns is to calculate the structure factor assuming a coherent source (t very small) and then convolute this expression with the measured resolution function. This requires no direct knowledge of the source width and hence has one less free parameter. The calculation of the structure factor and the convolution were performed numerically using MATHEMATICA. The results of such a procedure for both sizes of the pores and the same parameters as used earlier are shown in Fig. 4. The results are nearly identical to those obtained using the optical method of analysis that had a partially coherent source shown in Fig. 3.

This result suggests, not surprisingly, that the effects of the source are included in the resolution function. This must be the case as the resolution function is measured with the spectrometer aligned and all elements in place except the sample. This means that the resolution function, in a previously unexplored manner has included these source effects all along. Moreover, this explains why the resolution function is not the expected single Lorentzian. The results shown in Figs. 3 and 4 also indicate that incoherence of the source, along with the angular acceptance of the monochromator crystal, is a major factor requiring three Lorentzians to model the resolution function.

IV. CONCLUSIONS

The x-ray diffraction patterns on Anodisc filters with nominal pore diameters of 0.1 and 0.2 μm have been measured and analyzed. The patterns are consistent with pores of constant diameter and a Gaussian distribution of pore-pore spacing. The mean distance between pores, measured using x rays is 0.37 μm compared to 0.32 μm calculated from the nominal density of pores/cm^2. The results may be modeled both in terms of the convolution of a structure factor of the pores with the resolution function, and by modeling the source as a collection of incoherent sources. The two analysis techniques are indistinguishable. The incoherent source analysis provides the explanation for the need to model the resolution function by more than a single Lorentzian. The resolution function of a source with exponentially decaying spatial correlations and infinitesimal width is a Lorentzian. However, to obtain the resolution function of the whole source, this Lorentzian must be integrated over the width of the slit. With this knowledge, it is not surprising that a sum of Lorentzians, with all but one displaced from the origin, leads to a substantially better fit to the resolution function than a single Lorentzian.

ACKNOWLEDGMENTS

This work was partially supported by the National Science Foundation under Grant No. DMR89-20147, the ALCOM Science and Technology Center. M.R.F. wishes to thank Professor Harry C. Nash of John Carroll University for the discussions of Fourier optics.

APPENDIX: THE RESOLUTION FUNCTION

The effects of the finite coherence of the source and an effective source width roughly 10% of the physical width on the resolution function will be discussed in this appendix. The simple case of a one-dimensional exponentially decreasing correlation function in the plane of the source will be discussed. This is a reasonable model for behavior of spatial correlation functions.

The effects of a finite source on the measured resolution function are somewhat more complicated than the previous discussion. Following the standard approach [12], we note that the spectral density of the electron fluctuations $S(q,\omega)$ is the time and space Fourier transform of the electron-electron correlation function. At this stage, we will assume that the problem is essentially one dimensional. We further assume spatial correlation function in the monochromator crystal plane is a decaying exponential of the form $C(x) \propto \exp(-|x|/\zeta)$, where the correlation length is given by ζ. The differential intensity leaving the monochromator crystal is given by a modification of Eq. (1) and reads

$$dI(\theta) \propto \int_{-\infty}^{\infty} \exp[-|x|/\zeta]\exp[i(\theta+\xi/r)kx]dx\,d\xi = \frac{2\zeta d\xi}{1+k^2\zeta^2(\theta+\xi/r)^2}. \quad \text{(A1)}$$

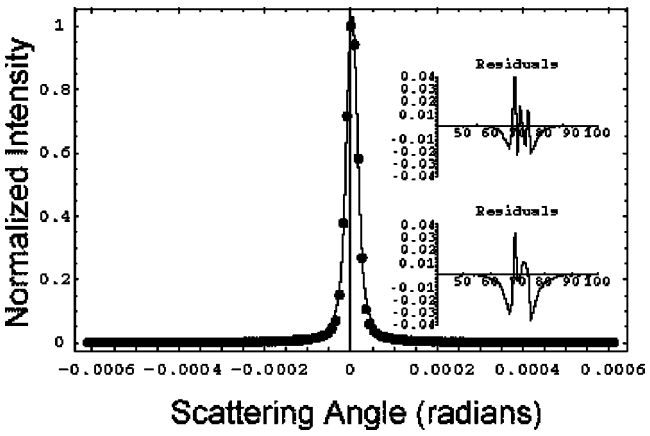

FIG. 5. The measured resolution function (points) and the fit (solid line) vs scattering angle. The top inset of the residuals is the arctangent form, while the lower inset shows the three Lorentzian form. The numbers on the inset refer to data point number, 0 corresponding to the far left and 140 corresponding to the far right.

This is an expression for a Lorentzian. This expression is readily integrated to obtain an analytic expression for $I(\theta)$. To do this one must integrate over the source slit. The resulting expression is

$$I(\theta) = \int_{-t}^{t} \frac{2\zeta d\xi}{1+k^2\zeta^2(\theta+\xi/r)^2} = \frac{2r}{k}\{\tan^{-1}[k\zeta(\theta+t/r)] - \tan^{-1}[k\zeta(\theta-t/r)]\}. \quad \text{(A2)}$$

This result can also be utilized to understand the shape of the resolution function in this experiment. It has been common knowledge for several decades that the resolution function measured in such spectrometers is significantly better fit to a sum of three Lorentzians rather than a single Lorentzian. This is in spite of the fact that a single Lorentzian is the expected form. While, the flat top of the Darwin width of the crystal has been suspected as the cause of this effect, there has been no previous analytic explanation of this result. However, Eq. (A2) the integral of a Lorentzian over the slit width also describes the resolution function. Figure 5 shows the measured resolution function, and fits to both the three Lorentzians and the sum of arctangent forms. The residuals are also displayed. An F test of the two fits indicates the arctangent form is a significantly better fit than the three Lorentzian form. The ratio of the χ^2's of the two fits lies in the tails of the F distribution. The value has a probability of occurrence greater than 2%. Furthermore, this form yields a value of the width $2t$ of 54 μm. This value is 10% less than that obtained from the fits to the pore diffraction patterns. Thus, by treating the monochromator as ideal and the source as incoherent the shape of the resolution function can be explained. Of course, all real crystals have an angular acceptance larger than zero. We believe that this is why the effective source width is smaller than the actual source.

[1] B.E. Warren, *X-ray Diffraction* (Addison-Wesley, Reading, MA, 1969). Also see A. Guinier and G. Fournet, *Small Angle Scattering of X-rays* (Wiley, New York, 1956).
[2] S.K. Sinha, *Liquid Crystals: Experimental Study of Physical Properties and Phase Transitions* (Cambridge University Press, Cambridge, 2001), Chap. 9, pp. 333–392.
[3] I.K. Robinson, special issue of Acta Crystallogr., Sect. A: Found. Crystallogr. **55**, 772 (1998).
[4] J. Ming (private communication).
[5] A. Primak, Ph.D. thesis, Kent State University, 2001.
[6] See, for example, Ref. [5] or Ref. [11].
[7] This is discussed in Ref. [14], p. 11. The data could not be fit to this form.
[8] This number was obtained from Whatman filters.
[9] L. Mandel and E. Wolf, *Optical Coherence and Quantum Optics* (Cambridge University Press, Cambridge, 1995), p. 149.
[10] J.W. Goodman, *Statistical Optics* (Wiley Interscience, New York, 1985). Also see L. Mandel and E. Wolf, *Optical Coherence and Quantum Optics* (Ref. [9]), pp. 148–150.
[11] B.M. Ocko, Ph.D. thesis, MIT, 1984.
[12] L. Mandel and E. Wolf, *Optical Coherence and Quantum Optics* (Ref. [9]), pp. 188–193; J.W. Goodman, *Statistical Optics* (Ref. [10]), pp. 207–216.
[13] L. Mandel and E. Wolf, *Optical Coherence and Quantum Optics* (Ref. [9]), p. 235.
[14] G.O. Reynolds *et al.*, *The Physical Optics Notebook: Tutorials in Fourier Optics* (SPIE Press, Bellingham, WA, 1989), p. 131. This is an application of the Fresnel-Kirchhoff diffraction formula discussed in M. Born and E. Wolf, *Principle of Optics*, 5th ed. (Pergamon Press, Oxford, 1975), p. 370.
[15] The model of fixed spacing $2b$ between slits might appear to be too gross a simplification. However, simulations in which the interference term is generated by slits of variable spacing with the spacing a Gaussian random variable indicate that the ''shoulders of the data'' can be modeled, but the secondary peaks only appear when the spacing variance is small, which approximates constant slit spacing.